pressure fluctuations because of the more corrugated interface causing the entrainment to occur at a lower critical velocity than a more flat-meshed interface. For a flat mesh with a relatively small value of L_1/L_2, the critical Weber number for entrainment will be higher. The viscosity group, $\mu_g/\sqrt{\rho_g \sigma L_1}$, accounts for the viscosity shearing action from the gas flow over the holding action of the interface due to the surface tension. Since for higher viscosity groups, the shearing action overrides the holding action, and the critical Weber number decreases with increasing magnitude of the viscosity group and entrainment will readily occur.

Droplet SMD

For the case of water-air interfaces, the measured droplet SMDs were regressed into Eq. (4) and a comprehensive correlation between the dimensionless Sauter mean diameter, SMD/L_1, and the other dimensionless parameters was determined:

$$\frac{SMD}{L_1} = 20.8283 \left(\frac{L_1}{L_2}\right)^{-0.392} \left(\frac{\rho_g V_{fg} L_1}{\mu_g}\right)^{-0.393} \left(\frac{\rho_g V_{fg}^2 L_1}{\sigma}\right)^{-0.349} \tag{6}$$

In this expression, the second and third terms on the right side represent Re_{L_1}, and We_{L_1}, based on L_1. Again, the last two dimensionless parameters in Eq. (4) for liquid-to-gas density and viscosity ratios were excluded since the present study did not consider variations of these parameters. The correlation shows that SMD/L_1 increases with decreasing L_1/L_2, Re_{L_1}, and We_{L_1}. The ratio of the entrained droplet SMD to a given L_1, will be high for a rough mesh with a smaller value of L_1/L_2, and will be low for a smoother mesh with a relatively large L_1/L_2. High Re_{L_1} and We_{L_1} imply that the inertial impact forces are dominant when compared to the viscous and the surface tension forces, respectively, and result in entrainment under stronger convective action. The entrained droplet SMD, therefore, shows a decrease with increasing Re_{L_1} and We_{L_1}. All the measured SMDs are plotted against the predicted values from the regression, Eq. (6), in Fig. 5. The data exhibited a good agreement with the regressed correlation with a maximum deviation of less than 10%.

Concluding Remarks

For the first time, two separate correlations for the entrainment onset velocity and the entrained droplet SMD were obtained from experimental data analyzed with the Buckingham-PI theorem. Saturated (or primed) mesh-laid interfaces between a water pool and a convective air stream was considered in an attempt to hydrodynamically simulate the entrainment phenomena in a heat pipe system. All the fluid properties were considered and/or evaluated at 1 atm and 20°C for the present case. If the results are applied to an operating heat pipe system at different temperatures, the constant A of both correlations must be modified in order to take into account the fluid property variations at the operational temperature of the individual heat pipes.

Acknowledgment

The authors would like to acknowledge the financial support provided by the National Science Foundation NSF Grant CTS-8922427.

References

[1]Peterson, G. P., "Thermal Control Systems for Spacecraft Instrumentation," *Journal of Spacecraft and Rockets*, Vol. 24, No. 1, 1986, pp. 99–101.

[2]Kihm, K. D., Kim, B. H., and Peterson, G. P., "Drop Size Measurements of Pool Entrainment Sprays from Mesh-Laid Surface," *Proceedings of the Institute of Liquid Atomization and Sprays*, (ILASS), San Ramon, CA, May 1992, pp. 234–239.

[3]Barth, H. G., *Modern Methods of Particle Size and Analysis*, Wiley, New York, 1984, pp. 135–172.

[4]Rosin, P., and Rammler, E., "The Laws Governing the Fitness of Powdered Coal," *Institute of Fuel*, Oct. 1933, pp. 29–36.

[5]Kihm, K. D., and Caton, J. A., "Synchronization of a Laser Fraunhofer Diffraction Drop Sizing Technique with Intermittent Spray System," *Applied Optics*, Vol. 31, No. 23, 1992, pp. 1914–1916.

[6]Kays, W. M., and Crawford, M. E., *Convective Heat and Mass Transfer*, 2nd ed., McGraw-Hill, New York, 1980, pp. 268–270.

[7]Buckingham, E., "On Physically Similar System: Illustrations of the Use of Dimensional Equations," *Physics Review*, Vol. 4, No. 4, 1914, pp. 345–376.

[8]Hinze, J. O., "Fundamentals of the Hydrodynamic Mechanism of Splitting in Dispersion Process," *AIChE Journal*, Vol. 1, No. 3, 1955, pp. 289–295.

Implicit Heat Pipe Vapor Model

W. Jerry Bowman* and Philip S. Beran†
Air Force Institute of Technology,
Wright-Patterson Air Force Base, Ohio 45433

Introduction

DIFFERENT approaches of numerically modeling transient heat pipe vapor phenomena have been developed and are reviewed in Ref. 1. Earlier models typically treat the vapor flow as one- or two-dimensional and compressible. This level of complication results in models that require large amounts of computer time to use. The vapor model studied in this Note is an extension of the model presented by Bowman et al.[1] Their one-dimensional model was different from previous models in that the vapor flow was assumed to be incompressible in space while still being compressible in time. Also, the vapor was assumed to be a saturated vapor, not an ideal gas. The assumption of spatially incompressible flow greatly simplified the model, thus greatly reducing the amount of computer resources needed to model a transient. The authors believe the saturated vapor assumption improves model accuracy. Vapor densities predicted from models that assume ideal gas behavior can deviate greatly from saturated vapor densities. Errors in predicting vapor density result in errors in predicting vapor velocity and pressure variations.

This Note improves on the model described in Ref. 1. A more accurate closure relationship relating vapor density to vapor temperature is used, and an implicit solution method is used to solve the governing equations. It is shown that the implicit solution is a factor 100 times faster than the earlier explicit solution method.

Governing Relationships

In order to model the vapor flow in a heat pipe, first an equation or system of equations that describe the physical

Received Oct. 13, 1992; revision received July 23, 1993; accepted for publication July 23, 1993. This paper is declared a work of the U.S. Government and is not subject to copyright protection in the United States.

*Associate Professor of Aerospace Engineering, Department of Aeronautics and Astronautics. Senior Member AIAA.

†Assistant Professor of Aerospace Engineering, Department of Aeronautics and Astronautics. Member AIAA.

situation in the vapor space must be developed. In Ref. 1 it is shown that conservation of mass for the vapor space is

$$\frac{\partial \rho}{\partial t} = \frac{2}{RL}\int_0^L (\rho_w V)\, dx \tag{1}$$

where ρ is the vapor density, t is time, R is the radius of the cylindrical vapor space, L is the length of the vapor space, and $\rho_w V$ is the mass flux leaving or entering the vapor space due to condensation or evaporation. The assumptions made during the development of Eq. (1) were 1) spatially constant vapor density, 2) cylindrical vapor space, and 3) azimuthal uniform evaporation and condensation rates.

The mass flux into the vapor space was modeled by applying conservation of energy to the interface between the vapor and the wick.[1] Conservation of energy can be written as:

$$h_{fg}(\rho_w V) = h(T - T_V) \tag{2}$$

where h_{fg} is the latent heat of evaporation, h is an evaporation/condensation coefficient, T is the temperature at the wick-vapor interface, and T_V is the vapor temperature. Finally, if Eq. (2) is substituted into Eq. (1), we obtain

$$\frac{\partial \rho}{\partial t} = \frac{2}{RL}\int_0^L \frac{h}{h_{fg}}(T - T_V)\, dx \tag{3}$$

In Eq. (3), two unknowns are present: 1) the vapor density and 2) the vapor temperature. The wick-vapor interface temperature T is a specified boundary condition for the vapor modeling problem. The evaporation/condensation coefficient h, and h_{fg}, are assumed to be known. For this work, h was assumed to be constant and have a value of 2500 W/m^2-K. In order to solve Eq. (3), a closure relationship is needed which relates vapor density to vapor temperature.

Closure will be provided by assuming the vapor is a saturated vapor. This is convenient because for a saturated vapor, temperature and density are dependent properties. Equation (4) is a general relationship between density and temperature for a saturated vapor[2]

$$\rho = \exp\left(\sum_{K=0}^{5} A_K T_V^K\right) \tag{4}$$

where the series coefficients A_K are constants for a specific working fluid found by curve fitting saturated vapor data (from Ref. 2, for T_V in K and density in kg/m^3, and for water, $A_0 = -68.622$, $A_1 = 0.52894$, $A_2 = -0.17525 \times 10^{-2}$, $A_3 = 0.31666 \times 10^{-5}$, $A_4 = -0.30147 \times 10^{-8}$, and $A_5 = 0.11981 \times 10^{-11}$).

Substituting Eq. (4) into Eq. (3) results in

$$\frac{\partial}{\partial t}\left[\exp\left(\sum_{K=0}^{5} A_K T_V^K\right)\right] = \frac{2}{RL}\int_0^L \frac{h}{h_{fg}}(T - T_V)\, dx \tag{5}$$

Two other useful relationships were used in studying the vapor flowfield. If conservation of mass is applied to a differential element in the vapor space, and if the flow is assumed to be instantaneously steady, the result is obtained

$$\frac{du}{dx} - \frac{2\rho_w V}{\rho R} = 0 \tag{6}$$

where u is the average local axial vapor velocity.

Similarly, if Newton's second law is applied to the same differential element, the result is obtained

$$\frac{dp}{dx} + \frac{d\rho u^2}{dx} + \frac{2\tau}{R} = 0 \tag{7}$$

where p is the local pressure and τ is the shear stress between the vapor and the wick. The shear stress can be modeled as

$$\tau = \frac{f\rho u^2}{2} \tag{8}$$

where f is a friction coefficient. A friction model which accounted for mass injection into or extraction from the vapor space was used.[3]

Solution Technique

We will now describe how these equations were numerically solved. The right side of Eq. (5) was numerically integrated using the trapezoidal rule:

$$\exp\left[\sum_{K=0}^{5} A_K (T_V^{n+1})^K\right] + \frac{\Delta th}{Rh_{fg}}\Theta T_V^{n+1} = \exp\left[\sum_{K=0}^{5} A_K (T_V^n)^K\right] + \frac{\Delta th}{Rh_{fg}}\left\{\frac{\Delta X}{L}\left[\Theta\left(\frac{T_1^{n+1} + T_{J\max}^{n+1}}{2} + \sum_{j=2}^{J\max-1} T_j^{n+1}\right) + (1-\Theta)\left(\frac{T_1^n + T_{J\max}^n}{2} + \sum_{j=2}^{J\max-1} T_j^n\right)\right] - (1-\Theta)T_V^n\right\} \tag{9}$$

Subscript j was used to represent different axial locations along the vapor space. In Eq. (9), T_V represents the vapor temperature (spatially constant), and $T_1, \ldots, T_j, \ldots, T_{J\max}$ represent the temperature of the vapor/wall interface which was not assumed to be spatially constant. In rewriting Eq. (5) to get Eq. (9), the right side of the equation is evaluated at an intermediate time through linear interpolation: the value of Θ specifies the time, the superscripts n and $n+1$ refer to present and future time levels, respectively. Setting Θ equal to 0 results in the right side of Eq. (5) being evaluated at the old time level (explicit formulation). Setting Θ equal to 1.0 results in the right side being evaluated at the future time level (fully implicit formulation). Selecting a value of Θ somewhere between 0 and 1 results in evaluating the term at an intermediate time level. For example, setting Θ equal to 0.5 results in evaluating the term at a time halfway between the present and the future time steps (Crank-Nicolson method).[4] At this value of Θ, Eq. (9) is a second-order accurate approximation to Eq. (5), $O[\Delta t^2]$, while for all other values the approximation is only first-order accurate, $O[\Delta t]$.

The only unknown in Eq. (9) is the temperature of the vapor at the future time level. All other variables are known or specified by the problem geometry and choice of working fluid. The values of the wick-vapor interface temperature T_j are specified for all locations along the vapor space and for all times during the transient in the form of a boundary condition. The temperature of the vapor at the new time step, T_V^{n+1} in Eq. (9), was computed using the bisection method.[4]

To arrive at a systematic means for choosing a time step when $\Theta < \frac{1}{2}$, we performed a linearized stability analysis of Eq. (9). In this analysis it was assumed that average wick-vapor interface temperature is constant. We found that for $\Theta < \frac{1}{2}$ a necessary condition for stability is

$$\Delta t \le \frac{2Rh_{fg}\dfrac{\partial \rho}{\partial T}}{h(1 - 2\Theta)} \tag{10}$$

The analysis also predicts unconditional stability for $\Theta \ge \frac{1}{2}$. For a heat pipe startup, Eq. (10) can be evaluated at the initial state to yield the most restrictive time step (assuming

Δt is held constant), since $\partial\rho/\partial T$ is smallest at the minimum operating temperature of the heat pipe.

Numerical Results

As a validation test, the model was used to simulate a heat-pipe vapor startup. The vapor space studied was cylindrical with a radius of 0.445 cm and a length of 0.691 m. One-fourth of the length corresponded to the evaporator end of the heat pipe, while the remainder was the condenser. Water was the working fluid. The vapor was assumed to initially be at rest in thermodynamic equilibrium with the walls of the heat pipe, all at a temperature of 340 K. At time equal to zero, the evaporator temperature began to rise until it reached 350 K. The condenser was maintained at 340 K.

Figure 1 compares three solution methods. All gave essentially the same results, although formal analysis predicts superior accuracy when $\Theta = \frac{1}{2}$. Because of the small time step size constraint when using the explicit method [0.0625 s for this example from Eq. (10)], the explicit method required 100 times more computer time than the implicit methods, $\Theta \geq \frac{1}{2}$, which were theoretically unconditionally stable and could use larger time steps. All methods used the same amount of computer time per time step.

Figure 2 illustrates the effect of axial grid spacing on solution accuracy. For all of the grid sensitivity studies, the Crank-Nicolson method was used with a time step of 2.5 s. As more grid points were used, the solutions converged. Figure 2 shows the axial pressure distribution along the heat pipe at time equal to 250 s into the transient. The figure is a graph of pressure drop from the end of the evaporator to any axial position, x. In Fig. 2, it can be seen that the pressure drops quickly through the evaporator due to friction and the acceleration of the vapor. An abrupt change in pressure is seen as the wall boundary condition changes from one of mass injection in the evaporator to one of mass extraction in the condenser. In the condenser, for this example, the pressure drop due to friction is almost entirely canceled by the pressure rise due to the deceleration of the vapor. The difference between the four solutions from the four grids is believed to be a result of different evaporator lengths for the different grids. For the 11 axial grid points solution, only 2 of the 11 grid points were in the evaporator (18% of the total length). For the 81 grid points solution, 20 of the grid points were in the evaporator (24.7% of the total length).

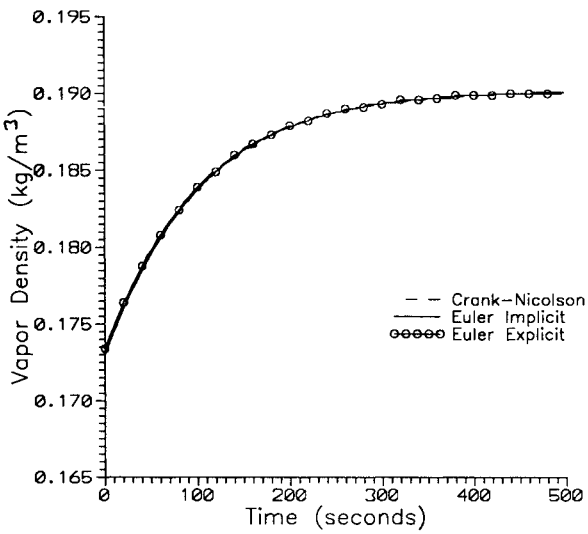

Fig. 1 Comparison of different solution methods.

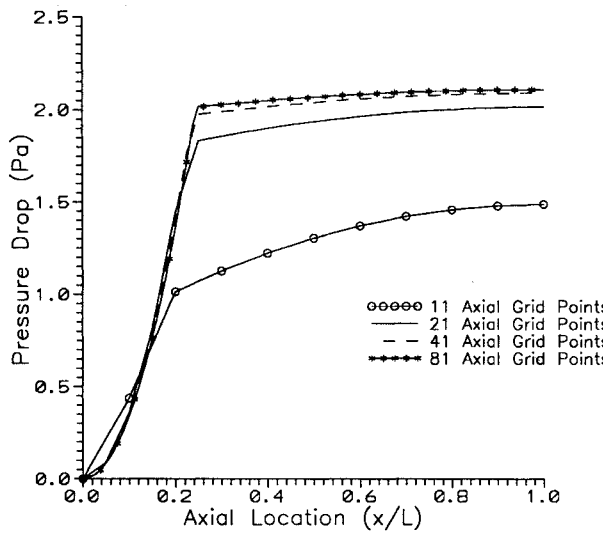

Fig. 2 Effect of axial grid on solution accuracy, Crank-Nicolson method.

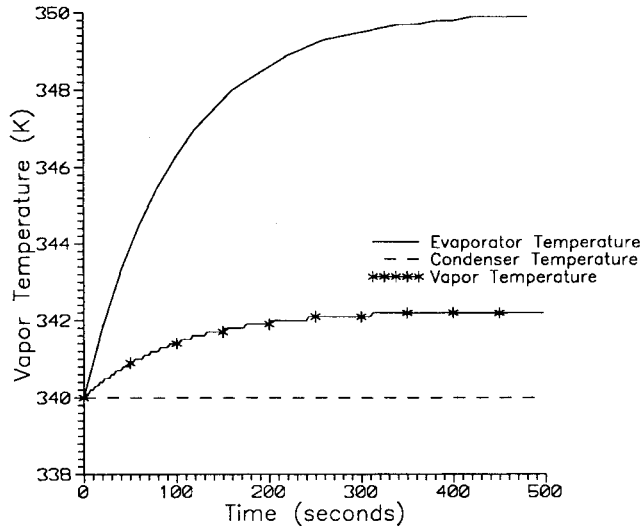

Fig. 3 Temperature variation during the transient.

Figure 3 is a graph of temperature during the transient. From the figure, it can be seen that vapor temperature rises during the transient and stays between the evaporator and condenser temperatures. The vapor temperature is closer to the condenser temperature because the condenser area is three times larger than the evaporator. Assuming the temperature results are accurate, the transient density results shown in Fig. 1 are believed to be accurate because they are simply a calculation based on the saturated vapor assumption [Eq. (4)]. The axial pressure data (Fig. 2) is not believed to be accurate. The accuracy of velocity or pressure results depends on accurate modeling of the evaporation and condensation processes. This can only be done if h is accurately known. The constant value for h for this work (2500 W/m^2-K) though ball park, is probably not accurate. More work is required in this area.

Conclusions

Two implicit solution methods for modeling vapor flow in a heat pipe were shown to be a factor of 100 times faster than an explicit solution method. All methods studied solved an identical set of governing equations and were shown to give the same results. The saturated vapor assumption made during the model development insured an accurate vapor density corresponding to the vapor temperature. The model was able to efficiently predict the transient behavior of the vapor density, temperature, velocity, and pressure, more information than is currently available from experimental data.

References

[1]Bowman, W. J., Winn, R. C., and Martin, H. L., "Transient Heat-Pipe Modeling, A Quasi-Steady, Incompressible Vapor Model,"

Journal of Thermophysics and Heat Transfer, Vol. 6, No. 3, 1992, pp. 571–574.

[2]Brenan, P. J., and Kroliczek, E. J., *Heat Pipe Design Handbook, Vol. II*, B&K Engineering, Inc., Towson, MD, June 1979.

[3]Bowman, W. J., and Hitchcock, J., "Friction Coefficients for Flow in Pipes with Mass Injection and Extraction," *Journal of Thermophysics and Heat Transfer*, Vol. 3, No. 1, 1989, pp. 92–94.

[4]Isaacson, E., and Keller, H. B., *Analysis of Numerical Methods*, Wiley, New York, 1966.

Reference Temperature Method and Reynolds Analogy for Chemically Reacting Nonequilibrium Flowfields

David J. Debrestian* and John D. Anderson Jr.†
University of Maryland,
College Park, Maryland 20742

Introduction

INTEREST in the development of a single-stage-to-orbit vehicle (SSTO) such as the National Aerospace Plane, and other advanced hypersonic vehicles such as waveriders,[1,2] has lent impetus to the need for more accurate engineering predictions for skin friction and heat transfer on such vehicles. These vehicles can be expected to operate in a flight regime (Mach: 5–25, altitude: 15–75 km), wherein nonequilibrium chemically reacting effects may be important. The reference temperature method, commonly used to approximate the skin friction coefficient, was developed for the flow of a calorically perfect gas[3–8] and later for equilibrium dissociated air.[9–11] Reynolds analogy, used in conjunction with the skin friction coefficient to approximate the Stanton number (St), and hence the heat transfer, shows a similar development for a calorically perfect[8] and an equilibrium gas.[9–11] The purpose of the present study is to assess the effectiveness of these two engineering approximations for nonequilibrium flowfield conditions.

Theory

A nonequilibrium chemically reacting flow is one in which finite rate chemical reactions dictate the chemical composition of the gas. For high-temperature air, dissociation and recombination (and perhaps ionization) are important. In chemically reacting flows, heat transfer rates become a dominant aspect, and in nonequilibrium flows various physical properties such as enthalpy, specific heats, and internal energy are functions of not only the temperature and pressure, but also of the "history" of the flowfield (via the nonequilibrium chemical composition).

The reference temperature method allows for the computation of skin friction coefficients for compressible flow by using classical results of incompressible flow. For example, for incompressible flow over a flat plate

$$c_f = (0.664/\sqrt{Re_x}) \tag{1}$$

One way Eq. (1) can be "corrected" for compressibility effects is by using

$$c_f \approx (0.664\sqrt{C^*}/\sqrt{Re_x}) \tag{2}$$

where Sutherland's law was used for C^*, given by

$$C^* = \left(\frac{T^*}{T_e}\right)^{1/2} \frac{T_e + K}{T^* + K} \tag{3}$$

In Eq. (3), K is a constant that depends on the gas considered. For this study, a value of $K = 250°\text{R}$ is used for molecular oxygen. Two equations used for T^* were compared in the present study

$$\frac{T^*}{T_e} = 1 + 0.032M_e^2 + 0.58\left(\frac{T_w}{T_e} - 1\right) \tag{4}$$

derived by Rubesin and Johnson,[3] and

$$\frac{T^*}{T_e} = 1.28 + 0.023M_e^2 + 0.58\left(\frac{T_w}{T_e} - 1\right) \tag{5}$$

from Young and Janssen,[4] who found this form of the equation to be more accurate for a calorically perfect gas for $M > 5.6$. As will be shown, Eq. (5) gave better results under the conditions considered for this study.

Reynolds analogy is a proportionality between St and the skin friction coefficient c_f, and can be expressed in the following form for flow over a flat plate:

$$St = \tfrac{1}{2}c_f Pr_w^{-2/3} \tag{6}$$

As the following explains, a range of different values for Pr_w and c_f were considered in this study.

Method of Analysis

It is unlikely that the reference temperature method would be accurate for a multispecies air model with a complex geometry if it did not prove effective for a simple reacting gas model/geometry configuration. For this reason, a flow of a binary mixture of atomic and molecular oxygen over a 10-ft flat plate was considered. (This work is now being extended by Ott[12] using a seven species air model over cone-derived "waverider" configurations.)

The boundary-layer equations for a two-dimensional, laminar, nonequilibrium chemically reacting binary mixture of atoms and molecules were solved with an implicit finite-difference scheme. In the interest of space, the details of the governing equations, chemistry, boundary-layer characteristics, and numerical method can be found in Ref. 13. This approach is patterned after that of Blottner.[14,15] Therefore, no further details will be given here.

Initial conditions for the nonequilibrium calculation in the form of velocity and temperature profiles were obtained by solving the boundary layer equations for the flow of a calorically perfect gas. For the specific case of flow over a flat plate, these equations are indeterminate at the sharp leading edge ($\xi, x = 0$) so the solution was carried out at a distance of 0.008 ft from the leading edge. Calorically perfect initial profiles close to the leading edge were considered sufficient since the flow is essentially frozen in that region. No difference in the downstream results was observed when either calorically perfect or nonequilibrium initial profiles were used.

The boundary condition at the outer edge of the boundary layer was chosen to be freestream conditions taken from Ref. 16. A constant temperature wall boundary condition was used as well as the assumption of an equilibrium fully catalytic wall. (Note: these results are not necessarily applicable for a noncatalytic or a partially catalytic wall.) The wall temperature

Received April 16, 1993; revision received July 6, 1993; accepted for publication July 26, 1993.

*Graduate Student, Aerospace Engineering; currently Member of the Technical Staff, Computational Physics, Inc., 2750 Prosperity Ave. #600, Fairfax, VA 22031. Member AIAA.

†Professor, Aerospace Engineering. Fellow AIAA.